

Document downloaded from:

<http://hdl.handle.net/10251/186992>

This paper must be cited as:

Carrión-Ruiz, B.; Riutort-Mayol, G.; Molada-Tebar, A.; Lerma, J.L.; Villaverde, V. (2021). Color degradation mapping of rock art paintings using microfading spectrometry. *Journal of Cultural Heritage*. 47:100-108. <https://doi.org/10.1016/j.culher.2020.10.002>



The final publication is available at

<https://doi.org/10.1016/j.culher.2020.10.002>

Copyright Elsevier

Additional Information

Highlights

- Color fading is not usually undertaken in rock-art archaeological sites.
- Microfading Tester (MFT) measurements is used to monitor the light-stability on spot samples.
- Gaussian processes are suitable to characterize and map spectral variations overtime.

Title: Color Degradation Mapping of Rock Art Paintings using Microfading Spectrometry

Author names and affiliations: Berta Carrión-Ruiz ^a, Gabriel Riutort-Mayol ^a, Adolfo Molada-Tebar ^a, José L. Lerma ^a, Valentín Villaverde ^b

^a*Department of Cartographic Engineering, Geodesy and Photogrammetry, Universitat Politècnica de Valencia, Valencia, Spain*

^b*Universitat de València, Departament de Prehistòria i d'Arqueologia, Blasco Ibáñez, 28, 46010 Valencia, Spain*

Corresponding author: Berta Carrión-Ruiz, bercarru@doctor.upv.es

Length of the manuscript: 6506 words.

Color Degradation Mapping of Rock Art Paintings using Microfading Spectrometry

Berta Carrión-Ruiz* ^a, Gabriel Riutort-Mayol ^a, Adolfo Molada-Tebar ^a, José L. Lerma ^a, Valentín Villaverde ^b

^aDepartment of Cartographic Engineering, Geodesy and Photogrammetry, Universitat Politècnica de València, Valencia, Spain

^bUniversitat de València, Departament de Prehistòria i d'Arqueologia, Blasco Ibáñez, 28, 46010 Valencia, Spain

Abstract

Rock art documentation is a complex task that should be carried out in a complete, rigorous and exhaustive way, in order to take particular actions that allow stakeholders to preserve the archeological sites under constant deterioration. The pigments used in prehistoric paintings present high light sensitivity and rigorous scientific color degradation mapping is not usually undertaken in overall archaeological sites. Microfading spectrometry is a suitable technique for determining the light-stability of pigments found in rock art paintings in a non-destructive way. Spectral data can be transformed into colorimetric information following the recommendations published by the Commission Internationale de l'Eclairage (CIE). The fading degree can be evaluated through the color changes produced, computing both color and chromatic differences. Microfading Tester (MFT) measurements on spot samples are time-consuming and difficult to materialize on-site. This paper presents the results of statistical Gaussian processes interpolation to map the potential MFT spectral variations overtime on a scene full of prehistoric rock art paintings. In addition, a descriptive analysis of color variations that may suffer the rock art motifs over time has been carried out. The advanced statistical methodology implemented can highlight potential changes on some rock support areas, and stable conditions on the painted red motifs over time, which can help to establish future conservation actions in the archeological site.

Keywords: Archaeology, Conservation, Open-air rock art, Microfading Tester (MFT), Gaussian processes, Digital camera

1. Research aims

In this study, the research aim is to perform an exhaustive descriptive analysis of potential color fading of pigment motifs and substrate over the entire surface of the rock art paintings on the Cova Remigia rock art shelter. Using Microfading Tester (MFT) color fading measurements and statistical interpolation based on a Gaussian process model for regression and prediction, it is possible to evaluate the potential changes in paintings.

2. Introduction

Spanish Levantine area holds open-air rock shelters with paintings on their walls. UNESCO included the Rock Art of the Mediterranean Basin as World Heritage in 1998. The undisputed protagonists of Levantine rock art paintings are humans, with anatomical features such as hair, nose and beard, all kinds of adornments, clothing, and equipment [1]. There is still a lack of knowledge about the conservation status of many archaeological sites, and how rock art is deteriorating [2]. Rock art paintings are suffering different types of actions, not only due to human activity but also natural weathering processes that affect the rock surface layers [3,4]. Especially, paintings of Levantine rock art environments are at risk: they are on surfaces that are exposed to rain, hail, dust, wind and intense sunshine.

It has been established that environmental conditions such as insolation as well as the geomorphological configuration of the host rock and the thermal distribution of the rock core influence the state of rock art paintings. These factors cause the erosion of the rocks and the degradation of the pigments due to the reaction of thermal shock and the changes in the chemical compounds of the paintings, consequence of the sunlight radiation received [5,6].

Studying and monitoring the long-term color change or fading behavior of these ancient materials is crucial to improve conservation [7]. The chemical and mineralogical composition of the pigments used, substrate, accretions, and alterations have been investigated during the last decades [8–10].

Nevertheless, the availability of efficient non-destructive assessment methods for conservation and research in rock art is limited. In most cases, it is necessary to take a sample, which alters and deteriorates rock art. The development of non-destructive methods for rock art assessment is therefore urgently required [4,6,11,12].

One of the most popular non-invasive techniques employed for conservation and prediction of spectral changes in paintings over time is microfading spectrometry. This is an accelerated aging method used for assessing the light-stability and prediction of color changes produced in materials over time. Research results show that it is a suitable technique to determine the light-fastness color variations in cultural heritage objects [6,13].

MFT offers many advantages. The instrument uses a robust non-destructive technique, since it allows measurements without direct contact with the material. Also, MFT enables evaluation of spectral changes in real-time, being a highly cost-effective technique [11,14]. MFT relies on the principle of reciprocity, applying a long light exposure and measuring the visible

1
2
3
4
5 reflectance spectrum of a small area, determining the color and its variation. Light sensitivity of a material can be obtained
6 from the spectral change as a perceptual measurement under testing conditions, after calculating either color differences or
7 chromatic differences using the CIELAB color space model [15].

8 Painting materials studied in museums with higher light sensitivity exhibit long-term color fading stabilization. They usually
9 experience rapid color changes at the beginning of the MFT measurements and, in a second stage, reach slowly their
10 maximum fading [16–19]. These studies helped users to predict the behavior of the analyzed pigments, however, depending
11 on their physicochemical characteristics the behavior can be different in each pigment. Long-term color fading stabilization
12 has been found in most of the light-sensitive colorants in museum collections.

13
14 For rock art sites with paintings, we need to register pictorial scenes as close as reality as possible [20]. Colorimetric
15 measurements can be used effectively to analyze color objects and their changes over time, monitoring the fading or the
16 damage of the pigments by light. For this purpose, calculating color differences between neighboring areas is recommended
17 in order to provide information about color degradation [11,21]. Color fading MFT observations on-site are difficult to set
18 up (hostile sites to be reached, rough panels, narrow ground, no electricity, etc.) and lengthy, thus, the number of punctual
19 time-series measurements is usually limited. Overcoming that limitation and estimating the color degradation of more
20 unmeasured points, could offer useful information for subsequent conservation actions. In order to achieve this a mapping of
21 potential MFT color variations on the surface over time has to be built. The mapping presented herein is the result of the
22 application of statistical model interpolation based on Gaussian processes for regression on the MFS data [22].

23
24 In this work, spectral measurements are focused on the Cova Remigia rock art shelter, province of Castellón, Spain. Some
25 authors, aware of the need for documentation and preservation of this archaeological site have contributed to these
26 purposes. Porcar et al. [23] and Sarriá Boscovich [24] were responsible for the first works of documentation of the motifs in
27 Cova Remigia. López-Montalvo et al. [25] applied energy dispersive X-ray fluorescence (EDXRF) technique and Raman
28 analysis to identify the Cova Remigia paintings and obtain chemical composition information. Del Hoyo-Meléndez et al. [6]
29 analyzed the photo-stability of the red and black pigments on two-spots of this rock art cave. Molada-Tebar et al. [26]
30 published a study on the color of the paintings using non-destructive digital photographic techniques. Other measurements
31 have already been made on this site on specific areas. In del Hoyo-Meléndez et al. [11] black and red samples on painted
32 motifs and the rock-support were selected, obtaining color degradation data. This paper confirmed that a high concentration
33 of pigment and dark red areas were more stable to light than areas with a thinner layer of pigment. However, the lack of
34 available information on their exact chemical composition as well as the variable environmental conditions can limit the
35 knowledge about future paintings' behavior. Thus, the assumption that this type of painted motifs can be from moderate to
36 very sensitive to lightfastness needs to be investigated.

37 Our novel approach presented herein can enrich previous studies undertaken by del Hoyo-Meléndez et al.[6,11], López-
38 Montalvo et al. [25] and Roldán et al. [27] on this rock art shelter.

39
40 The rest of the paper is structured as follows. Section 3 briefly describes the materials of study, instrumentation and calculus
41 applied. Section 4 describes the resulting predicted color fading figures (mapping) as well as a discussion about the results
42 obtained. Finally, Section 5 draws some conclusions.

43 **3. Materials and Methods**

44 *3.1. Archaeological site and sample materials*

45
46 Cova Remigia is considered one of the relevant sites of Levantine rock art due to its large number of motifs and the
47 exceptionality of these in terms of composition and stylistic design [24,25]. Those motifs are located in the opened-air rock
48 shelter number V of Cova Remigia (Figs. 1 and 2a) in Ares del Maestrat, Castellón, Spain. Cova Remigia archaeological site
49 integrates 6 shelters (summing up to 20 m length, 9 m depth and 7 m height).

50
51 Several characteristics of the location and morphology of the shelter were taken into account to select the most favorable
52 testing conditions. On the one hand, the measurement campaigns were taken considering the illumination changes that suffer
53 the place during the day. Paintings received direct morning sunlight per day, between two and three hours. The sunlight
54 reception time varied between 7:30 and 10:30 am. On the other hand, the walls presented an irregular surface, high number
55 of motifs (Fig. 2a), and the setup of the MFT employed became rather difficult, complicating the acquisition time for each of
56 the sampling spots.
57
58
59
60
61
62
63
64
65

1
2
3 The materials investigated included series of pigments applied to the rock substrate. Previous works established that the area
4 of study contains motifs of different phases [24]. The set of samples taken was constrained to a rock art hunting scene that
5 combines several humans (but only two were analyzed in this work, samples 3, 4 and 12) and animal motifs, two wild boars
6 (samples 6 and 7)), and others humans figures, probably added later, which not participated in the hunting scene (samples 1
7 and 5). Information and a general description of the samples surveyed in this study are presented in Table 1 and Fig. 2. In
8 addition, the initial coordinates of the sample points are displayed in a chromaticity diagram (Fig. 3)
9

10 The basic raw material of Cova Remigia paintings has been identified as iron oxide (haematite) in a limestone calcareous
11 rock surface. Additional information about the chemical composition of the same archaeological site (Valltorta-Gasulla area)
12 can be found in [25]. Furthermore, the previous MFT measurements have been used in Cova Remigia to determine the
13 sensitivity to light in the chosen spots [11].
14

15 **3.2. Instrumentation**

16 **3.2.1. MFT Display**

17 The MFT is a non-destructive method that estimates the fading rates of colored surfaces [28] and can be used to assess the
18 risk of light damage on surfaces. The device system consists of a high-power solid-state plasma light source that illuminates
19 an approx. 0.5 mm spot on the object with an intensity of 6.0 Mlx, 0°/45° geometry optical setup, and a VIS reflectance
20 spectrometer [29].
21

22 The MFT emits visible light to simulate the lighting conditions on-site. The range from the lens to the surface of the sampling
23 spot is approximately 1.0 cm (Fig. 4).
24

25 MFT time-series of observations represent potential spectral response changes [6,11,13,30]. MFT setup is highly sensitive to
26 variations in movement, surface, and, last but not least, lighting conditions, so observations reflect usually large fluctuations
27 and noise. In this case, changes are expressed either in color differences (ΔE) or in chroma differences (ΔC) over time. These
28 measurements are observed on the surface of the material under study, under difficult and time-consuming setups
29 (approximately 20 minutes per spot).
30

31 **3.2.2. Photographic setup**

32 To obtain the color values of the sampling spots, the rock art paintings were recorded with a digital camera. The digital
33 camera used was a Fujifilm IS Pro. This single-lens reflex (SLR) camera is specific for the realization of medical and scientific
34 photography and uses a Super CCD sensor. The quality of the photographs depends on the use of adequate optics too. In our
35 case, a quartz lens, Coastal Optical UV-VIS-IR Apo Macro of 60 mm, we attached to the SLR camera body.
36
37

38 **3.3. Color and chromatic differences calculations**

39 Two different types of MFT data are analyzed: MFT data based on color differences and MFT data based on chroma
40 differences. The spectral reflectance data obtained by the MFT can be transformed into colorimetric information following
41 the recommendations published by the Commission Internationale de l'Éclairage [15,31–33].
42

43 CIELAB color space is a suitable option to measure the color of the rock art motifs because it is a color space close to human
44 visual perception. When a color is expressed in CIELAB, L^* defines lightness, a^* denotes redness-greenness and b^* the
45 yellowness-blueness.
46

47 A recommended way to calculate the color difference between samples from a colorimetric reference is through its Euclidean
48 distance using the equation known as Delta E, CIE76 or ΔE_{ab}^* [15]. CIE76 is used instead of other more recent formulas for
49 calculating the color differences (Eq. 1) because it is more suitable for archaeological applications [34]. However ΔE_{ab}^*
50 indicates only the total magnitude of a color difference, but do not necessarily show the direction of this difference. It is more
51 interesting to analyze the information provided separately by each of the components. The variations in CIELAB parameters
52 permit to evaluate the magnitude and direction of the color changes.
53
54

$$55 \Delta E_{ab}^* = \sqrt{(\Delta L^*)^2 + (\Delta a^*)^2 + (\Delta b^*)^2} \quad (1)$$

56
57 However, another option to obtain ΔE_{ab}^* is using the CIELCH coordinates. It is a closer way, as our brain interprets and
58 conceptualizes the signals received through visual stimulus. The main advantage of using CIELCH rather than CIELAB is
59 that we can describe a color using its three perceptual attributes, i.e. Hue (H^*), Chroma (C^*) and Lightness (L^*). Accordingly,
60 another way to obtain ΔE_{ab}^* is using the CIELCH coordinates (Eq. 2):
61
62
63
64
65

$$\Delta E_{ab}^* = \sqrt{(\Delta L^*)^2 + (\Delta C)^2 + (\Delta H)^2} \quad (2)$$

It is important to note that color differences lower than 2.3 are not noticeable by the naked eye in the CIELAB (1976) color space [35]. Thus, color differences below 3 CIELAB units, will be considered insignificant since they are not perceptible to the human eye.

The lightness value (L^*) is achromatic since it describes its relative brightness or luminous intensity. Therefore, the analysis of chromatic characteristics through the C^* value can be interesting for this study. As defined by the CIE [15], chroma describes the vividness or dullness of a color, i.e. the chromatic strength of object color. As color becomes progressively desaturated, it will gradually lose its identity. Brilliant, vivid, intense colors are achieved with high levels of saturation. For an object to have high chroma, it must reflect/transmit one or two parts of the spectrum very strongly and the rest very weakly. The Chroma value of each feature can be obtained thus with Eqs. 3 and 4:

$$C_1^* = \sqrt{a_1^2 + b_1^2} \quad (3) \quad C_2^* = \sqrt{a_2^2 + b_2^2} \quad (4)$$

The Chroma difference is calculated as follows (Eq. 5):

$$\Delta C_{ab}^* = C_2^* - C_1^* \quad (5)$$

In that way, high Chroma values represent more vivid colors than low Chroma values. That is, positive chroma differences mean that the color becomes brighter, and negative chroma differences mean that the color of the study becomes duller and less bright.

3.4. Interpolation method

3.4.1. Data description

The data set consists of MFT time-series (with $T = 11$ -time points, $t = 1, \dots, T$) targeting $N = 13$ spatial sampling spots ($i = 1, \dots, N$) of the rock art scene and two other human figures not integrated into the hunting scene (Fig. 2b and Table 1). This spatiotemporal collection of MFT observations is denoted as \mathbf{y} .

To evaluate the interpolation model, additional covariates as input variables have to be used. In this regard, image color values are used as input variables to build and evaluate the correlation [36]. Hence, image color variables H (Hue), S (Saturation), I (Intensity) jointly with the X and Y spatial coordinates (pixel coordinates) and time for every sampling and predicting points are used as inputs in the interpolation model (Table 2).

3.4.2. Interpolation method

The mapping presented herein is the result of the application of an interpolation statistical model based on Gaussian processes for regression and prediction. A Gaussian process model is a powerful and flexible non-parametric model for D -dimensional (e.g. spatial and temporal dimensions) functions with multivariate predictors (inputs variables) in each dimension. The main element of Gaussian processes is the covariance function which evaluates the correlation structure between observations as a function of the inputs variables in D -dimensional space. The covariance function is a key element to make reliable predictions since it encodes the covariance structure of function values [37].

In [22] and [38] the authors evaluated the performance of using a multivariate Gaussian process model for predicting new MFT data. Also, they included the derivatives of the Gaussian process model to constrain the model to meet the properties of monotonicity and long term-stabilization of MFT color variations over time. Next, the basics of this model are described. The model is $\mathbf{y} = \mathbf{f} + \boldsymbol{\epsilon}$, where \mathbf{f} is the latent function underlying the MFT noisy observations \mathbf{y} , and $\boldsymbol{\epsilon}$ is the Gaussian noise term. Thus, the likelihood function can be expressed as follows:

$$\mathbf{p}(\mathbf{y}|\mathbf{f}) = \text{Normal}(\mathbf{y}|\mathbf{f}, \sigma^2), \quad (6)$$

with Gaussian noise variance σ^2 . The latent function \mathbf{f} is modeled as a Gaussian process:

$$\mathbf{f} \sim \text{Normal}(\mathbf{0}, \mathbf{K}),$$

where \mathbf{K} denotes the covariance matrix evaluated by a squared exponential covariance function $k(\mathbf{x}, \theta)$ [37] as a function of covariance parameters θ and input values $\mathbf{x} = [H, S, I, X, Y, \tau]$, with τ denoting the time points, such that the element (i, t) of \mathbf{K} is given by the covariance function k evaluated at the corresponding input values \mathbf{x}_{it} :

$$\mathbf{K}_{it} = k(\mathbf{x}_{it}, \theta).$$

The constraints of monotonicity and long term stabilization of the predicted functions are included in the likelihood function through additional observations [22,39]. Thus, the likelihood model in Eq. 6 is extended to consider the virtual derivative constraining observations for monotonicity \mathbf{z} and long term stabilization \mathbf{y}' as follows:

$$p(\mathbf{y}, \mathbf{z}, \mathbf{y}' | \mathbf{f}, \mathbf{f}') = \text{Normal}(\mathbf{y} | \mathbf{f}, \sigma^2) \Phi\left(\mathbf{z} \cdot \mathbf{f}' \cdot \frac{1}{v}\right) \delta(\mathbf{y}' - \mathbf{f}'), \quad (7)$$

where \mathbf{f}' is the corresponding latent function values to the derivative observations \mathbf{z} and \mathbf{y}' . In the previous joint likelihood function in Eq. 7, the term $\Phi\left(\mathbf{z} \cdot \mathbf{f}' \cdot \frac{1}{v}\right)$ is the Probit likelihood function for the virtual derivative observations for monotonicity \mathbf{z} (with $\mathbf{z}_i \in (1, -1)$; $\mathbf{z}_i = 1$ for positive derivative and $\mathbf{z}_i = -1$ for negative derivative) with parameter v controlling the strictness of the constraint. And the term $\delta(\mathbf{y}' - \mathbf{f}')$ is the Dirac Delta likelihood function for the virtual derivative observations $\mathbf{y}' = 0$ for long term stabilization. The joint distribution of regular \mathbf{f} and derivative \mathbf{f}' latent function values is:

$$\begin{pmatrix} \mathbf{f} \\ \mathbf{f}' \end{pmatrix} \sim \text{Normal}\left(\mathbf{0}, \begin{pmatrix} \mathbf{K}_{ff} & \mathbf{K}_{ff'} \\ \mathbf{K}_{f'f} & \mathbf{K}_{f'f'} \end{pmatrix}\right),$$

where the covariance matrix has been extended to include the covariances between observations and partial derivatives ($\mathbf{K}_{ff'}$ and $\mathbf{K}_{f'f}$) and the covariances between partial derivatives ($\mathbf{K}_{f'f'}$) (see [22] and [39] for the math expressions of the derivative covariance functions). More details about this Gaussian process model with monotonicity and long term stabilization constraints can be found at [22] and [38].

In the present paper, we implemented this model using the GPy toolbox2 (GPy: A Gaussian process framework in Python. <https://sheffieldml.github.io/GPy/>, since 2012) which besides the regular Gaussian process includes gradients of the Gaussian process (<https://github.com/SheffieldML/GPy/pull/678>). Employing this implementation the model was fitted and predictions for mapping over space and time of potential color variations on the surface of rock art paintings were obtained.

Finally, a complete map of the estimated color fading data for the entire surface under study is worth-valued information to achieve further successful conservation actions. In the next section, estimated color fading mappings are presented as results of the interpolation of MFT.

4. Results

The measured color differences and chroma differences at each time are presented as cross points in Fig. 5 and Fig. 6, respectively. Furthermore, solid lines represent the model prediction of chroma/color change evolution per sample over time.

Fig. 5 shows the predictive means (solid line) and the errors in the predictions (dotted line), on the set of training MFT data (Fig. 2b, cross points) based on color differences over time. The results are plotted and split (a, b, c) to improve their visibility and understanding. Resulting ΔE_{ab}^* curves provide a quantitative way of assessing the behavior of the measured spots over time. According to these results, sampling spots 9 (Fig. 5a), 10 (Fig. 5b), and 13 (Fig. 5c) show color differences higher than 3 units referred to T observations over 4, being close to 6 units at spots 9 and 10, and close to 4 units at sampling spot 13. The remaining sampling spots have ascending curves in terms of the color difference values over time. However, for the highest T values, color differences remain below 3 units. In this way, sampling spots 1 (Fig. 5a), 6 (Fig. 5b) and 8 (Fig. 5c) have ΔE_{ab}^* values ranging 2-3 units, whereas sampling spots 2 and 3 (Fig. 5a), 4, 5 and 12 (Fig. 5b), and 7 and 11 (Fig. 5c) reach values very close to 1 unit.

Fig. 6 shows the predictive means (solid lines and the errors in the predictions (dotted lines), on the set of training MFT data (Fig. 2b, cross points) based on chroma differences over time. As set out above, the results are plotted and split (a, b, c). The behaviors of the samples in terms of chroma and color differences are pretty similar over time. Sampling spots 9 (Fig. 6a), 10 (Fig. 6b), and 13 (Fig. 6c) show color differences higher than -2 units for the highest T values. In particular, almost -4 units at spots 9 and 13, and slightly higher than -2 units at point 10. Regarding the rest of the samples, chroma differences remain fairly stable, between the intervals -1 and 1. Except for samples 1 (Fig. 6a) and 6 (Fig. 6b) that have values slightly higher than 1 unit and -1 unit, respectively.

5. Discussion

According to these results, the color degradation of rock art paintings can be classified into two groups based on their spectral response changes. Firstly, sampling spots 9, 10 and 13 which are in the most variable areas, i.e. with highest values of color differences and chromatic differences, which correspond with rock support areas. Secondly, the rest of the sampling points do have color differences and chroma differences that are quite stable over time since they do not reach significant values.

To make continuous color fading maps over the rock art scene, predictions of color fading curves have been computed for all the spatial pixel locations. Fig. 7 represents the spatial distribution and their evolution over time for those color fading estimates based on ΔE_{ab}^* . The images correspond to the time points $t = 3$, $t = 4$, $t = 5$, $t = 6$ and $t = 11$. Similarly, Fig. 7 shows the color fading estimates based on the chromatic differences.

Overall, color differences mapped reveal that the maximum color change is given at the top of the map (Fig. 7). This area corresponds mostly with rock support. Likewise, chroma differences mapped results (Fig. 8) corroborate the results obtained in the map based on the color differences, i.e. there is no loss of color and the most unstable area is the one above the map displayed in blue and purple tones.

Furthermore, five specific spots of the studied paintings are analyzed (Fig. 9). The chosen spots correspond to areas of high chromatic differences, positive differences in the case of pigment pixels, and negative differences in the case of the substrate pixel. The selection consists of 4 points in each painted figure and 1 point on the rock-support. Two of them are part of the hunting scene figures (spots 2 and 4 in Fig. 9, which corresponds to the two wild boars) and the others (spots 1 and 3 in Fig. 9) are part of figures added probably later, because they present a different style and for that reason, they were not represented as part of the hunting scene of the 5th cavity in the study of this scene carried out by Sarriá Boscovich [24].

A complete description of the spots displayed in Fig. 9 is presented in Table 3. To show the evolution of the chroma differences in those specific areas, Fig. 10 shows the track of the selected pixels in each measured time. Besides, the color changes can be better appreciated by plotting the chromatic changes as in Fig. 8. It is interesting to note that although the pigment areas do not reveal significant chromatic changes, the areas with higher chromatic changes, around 2 units (mapped in dark red) correspond with the surrounding areas of samples 1, 5, and 13. On the other hand, the areas mapped in blue/purple (chromatic changes around -3 units) correspond with rock support areas. Regarding this issue, spot 5 in Fig. 10 reveals that chroma differences increases and color becomes duller over time.

As pointed out above, the color becomes brighter if chroma differences are positive, and duller if they are negative. Therefore, the results reveal that the painted motifs become brighter as time increases. On the contrary, the areas of rock-support become faded as time increases. Therefore, it would be interesting to apply conservation actions in these areas. Also, environmental factors such as wind erosion, weathering conditions or lichens can affect those predictions and must be taken into account too.

Contrasting the results obtained, there are no significant spectral changes in the painted areas. According to del Hoyo-Meléndez et al. [11], the spectral response variability in the dark red art areas remains low over time. Values around 3 units of color difference are reached and mapped in yellow or light green (Fig. 9) and values around 1 unit of chroma difference are mapped in red (Fig. 8). As well as spots 2, 3, and 4 in Fig. 9 are plotted in the range between 1 and 2 (red and dark red bands) for most of the time studied in Fig. 10.

On the one hand, the higher color difference value is registered in the front legs of the central motif, since this area shows a change of color close to 6 units (dark orange areas). Therefore, that area can be identified as the highest variable painted area analyzed. However, chroma differences are close to 1 unit as it is displayed in spot 4 (Fig. 10). On the other hand, Fig. 10 displays that the highest chroma difference values are registered in the surroundings of spots 1 and 3 in Fig. 9. Reaching this point, it is important to analyze the reason for this variability. Firstly, it is known that red rock art paintings are Fe-based and Fe-based pigments generally exhibit good lightfastness properties as Druzik [41] obtained in the pigments samples of their research. This explains that the spectral changes obtained for the painted areas are not excessively significant in any area.

However, it is important to note that spots 1 and 3 of Fig. 9 are located in motifs added in different phases of execution than the rest, spots 3, 6, 7, and 12 in Fig. 2b. These differences might ratify the stylistic differences observed by Sarriá Boscovich [24], despite we are analyzing herein only the color fading.

The spectral change could also be due to the singularities of rock support. MFT only offers physical information, hence other techniques such as EDXRF or Raman should be applied to obtain a characterization of the pigments and strengthen the

1
2
3 previous hypothesis.
4
5

6. Conclusions

6
7

8 The MFT data was employed to estimate color fading on a rock art paintings from Cova Remígia (Castellon, Spain) after
9 analyzing the spectral response behavior of the whole scene. The results allow us to confirm that the colorimetric variables
10 are useful for correlating MFT and digital imagery data, as well as making predictions on color-fading curves for new non-
11 observed locations. Therefore, predicted values over time, namely, their spectral response changes, yield worth-valued
12 information to set further conservation actions and successful preventive conservation measures and guidelines.

13 Temporal evolution mapping on rock art scenes suggests that red motifs will not change significantly over time. However,
14 some areas of the rock-support are susceptible to color changes/degradation over time. The most potentially affected areas
15 are those were the highest chroma differences were achieved (bluish and purplish areas). Thus, it can be concluded that cave
16 paintings may have a potential risk of damage due to the degradation of the rock-support.

17 Rock art motif colors are challenging to identify and preserve inside archaeological sites due to their variable compositions,
18 substrates, and environmental conditions. For that reason, these effects may vary between and within rock art archaeological
19 sites, so it is recommended to perform the study of color degradation in local zones for each of the scenes, and avoid
20 extrapolation.

21 Moving forward, it is highly recommended to plan carefully where the sampling spots should be layout in the scene, taking
22 into consideration not only physicochemical features and proper MFT setup, but also environmental factors and
23 archaeological knowledge in order to give answers to open archeological questions such as scene composition, stylistic
24 variations and drawing execution phases. In the future, we would like to integrate meteorological data and sunlight hitting
25 hours to estimate the right equivalency between the exposure time that applies for the MFT measurements and the true
26 sunlight exposure received.
27
28

Acknowledgments

29
30

31 *The authors would like to thank the Generalitat Valenciana for providing access to the site during the measurement*
32 *campaigns and Dr Julio del Hoyo-Meléndez from the National Museum in Krakow for providing the MFT. Also thanks to the*
33 *Probabilistic Machine Learning Group in Aalto University for helping with the GPy implementation of the model. Input from*
34 *the archeologist Dra Esther López-Montalvo is also gratefully acknowledged. This research was partially supported by*
35 *Research and Development Aid Program PAID-01-16 from the Universitat Politècnica de València [FPI-UPV-2016 Sub I*
36 *grant].*
37

REFERENCES

38
39

- 40
41 [1] I. Domingo, Art primer. Artistes de la prehistòria, Museu d'Arqueologia de Catalunya, 2020.
42 [2] M.J. Giesen, A. Ung, P.A. Warke, B. Christgen, A.D. Mazel, D.W. Graham, Condition assessment and preservation of open-air rock art panels
43 during environmental change, *J. Cult. Herit.* 15 (2014) 49–56. doi:10.1016/j.culher.2013.01.013.
44 [3] K. Hall, I. Meiklejohn, P. Sumner, J. Arocena, Light penetration into Clarens sandstone and implications for deterioration of San rock art,
45 *Geoarchaeology.* 25 (2010) 122–136. doi:10.1002/gea.20296.
46 [4] L. Mol, H.A. Viles, Geoelectric investigations into sandstone moisture regimes: Implications for rock weathering and the deterioration of San
47 Rock Art in the Golden Gate Reserve, South Africa, *Geomorphology.* 118 (2010) 280–287. doi:10.1016/j.geomorph.2010.01.008.
48 [5] A. Díez-Herrero, I. Gutiérrez-Pérez, J. Lario, J.C. Cañaveras, D. Benavente, S. Sánchez-Moral, J. Alonso-Azcárate, Analysis of potential direct
49 insolation as a degradation factor of cave paintings in Villar del Humo, Cuenca, Central Spain, *Geoarchaeology.* 24 (2009) 450–465.
50 doi:10.1002/gea.20274.
51 [6] J.M. del Hoyo-Meléndez, J.L. Lerma, E. López-Montalvo, V. Villaverde, Documenting the light sensitivity of Spanish Levantine rock art
52 paintings, *ISPRS Ann. Photogramm. Remote Sens. Spat. Inf. Sci.* II-5/W3 (2015) 53–59. doi:10.5194/isprsannals-II-5-W3-53-2015.
53 [7] M. Cassar, P. Brimblecombe, T. Nixon, C. Price, C. Sabbioni, S. Jimenez, K. Van Balen, Technological requirements for solutions in the
54 conservation and protection of historic monuments and archaeological remains, 2001.
55 [8] E. López-Montalvo, C. Roldán, E. Badal, E. Murcia, V. Villaverde, First identification of plant cells in prehistoric black pigments of Spanish
56 Levantine rock art by means of a multi-analytical approach: chaine opératoire and cultural assessments., *PlosOne.* (2017) 1–27.
57 doi:10.1371/journal.pone.0172225.
58 [9] M.Á. Rogerio-Candelera, P. Bueno Ramírez, R. de Balbín-Behrmann, M.I. Dias, L. García Sanjuán, M.L. Coutinho, J.A. Lozano Rodríguez,
59 A.Z. Miller, A.W. Pike, C.D. Standish, M.I. Prudêncio, A.L. Rodrigues, J.M. De la Rosa Arranz, D. Gaspar, Landmark of the past in the
60 Antequera megalithic landscape: A multi-disciplinary approach to the Matababras rock art shelter, *J. Archaeol. Sci.* 95 (2018) 76–93.
61 doi:10.1016/j.jas.2018.05.005.
62
63
64
65

- 1
2
3
4
5 [10] C. Roldán García, V. Villaverde Bonilla, I. Ródenas Marín, S. Murcia Mascarós, A unique collection of Palaeolithic painted portable art: Characterization of red and yellow pigments from the Parpalló Cave (Spain), *PLoS One*. 11 (2016) 1–22. doi:10.1371/journal.pone.0163565.
- 6 [11] J.M. del Hoyo-Meléndez, B. Carrión-Ruiz, G. Riutort-Mayol, J.L. Lerma, Lightfastness assessment of Levantine rock art by means of
7 microfading spectrometry, *Color Res. Appl.* (2019) 1–9. doi:10.1002/col.22372.
- 8 [12] I. Domingo, B. Carrión, S. Blanco, J.L. Lerma, Evaluating conventional and advanced visible image enhancement solutions to produce digital
9 tracings at el Carche rock art shelter, *Digit. Appl. Archaeol. Cult. Herit.* 2 (2015) 79–88. doi:10.1016/j.daach.2015.01.001.
- 10 [13] J.M. del Hoyo-Meléndez, M.F. Mecklenburg, A survey on the light-fastness properties of organic-based Alaska Native artifacts, *J. Cult. Herit.*
11 11 (2010) 493–499. doi:10.1016/j.culher.2010.01.004.
- 12 [14] B. Ford, Non-destructive microfading testing at the National Museum of Australia, *AICCM Bull.* 32 (2011) 54–64.
13 doi:10.1179/bac.2011.32.1.008.
- 14 [15] CIE, CIE 015:2004. Colorimetry, 3rd ed., Commission Internationale de l’Eclairage, 2004. [http://www.cie.co.at/publications/colorimetry-3rd-](http://www.cie.co.at/publications/colorimetry-3rd-edition)
15 [edition.](http://www.cie.co.at/publications/colorimetry-3rd-edition)
- 16 [16] C.H. Giles, The fading of colouring matters, *J. Appl. Chem.* 15 (1965) 541–550.
- 17 [17] C.H. Giles, D.P. Johari, C.D. Shah, Some observations on the kinetics of dye fading, *Text. Res. J.* 38 (1968) 1048–1056.
- 18 [18] R. Johnston-Feller, C. Bailie, M. Curran, The kinetics of fading: opaque paint films pigmented with alizarin lake and titanium dioxide, *J. Am.*
19 *Inst. Conserv.* 23 (1984) 114–129.
- 20 [19] R.L. Feller, R. Johnston-Feller, C. Bailie, Determination of the specific rate constant for the loss of a yellow intermediate during the fading of
21 alizarin lake, *J. Am. Inst. Conserv.* 25 (1986) 65–72.
- 22 [20] J.F. Ruiz, J. Pereira, The colours of rock art. Analysis of colour recording and communication systems in rock art research, *J. Archaeol. Sci.* 50
23 (2014). doi:10.1016/j.jas.2014.06.023.
- 24 [21] F. Boochs, A. Bentkowska-kafel, C. Degriigny, M. Karaszewski, A. Karmacharya, Z. Kato, M. Picollo, A. Sciences, L.H. Str, Colour and Space
25 in Cultural Heritage : Key Questions in 3D Optical Documentation of Material Culture for Conservation , Study and Preservation Spectral
26 Object Documentation : Questions of Colour, (2014) 11–24.
- 27 [22] G. Riutort-Mayol, M.R. Andersen, A. Vehtari, J.L. Lerma, Gaussian process with derivative information for the analysis of the sunlight adverse
28 effects on color of rock art paintings, (2019) 1–16. <http://arxiv.org/abs/1911.03454>.
- 29 [23] J.B. Porcar, H. Obermaier, H. Breuil, Excavaciones en Cueva Remigia (Castellón), Madrid, España., 1935.
- 30 [24] E. Sarriá Boscovich, Las pinturas rupestres de Cova Remigia (Ares del Maeste, Castellón), *Lucentum An. La Univ. Alicant. Prehist. Arqueol. e*
31 *Hist. Antig.* (1988) 7–34.
- 32 [25] E. López-Montalvo, V. Villaverde, C. Roldán, S. Murcia, E. Badal, An approximation to the study of black pigments in Cova Remigia
33 (Castellón, Spain). Technical and cultural assessments of the use of carbon-based black pigments in Spanish Levantine Rock Art, *J. Archaeol.*
34 *Sci.* 52 (2014) 535–545. doi:10.1016/j.jas.2014.09.017.
- 35 [26] A. Molada-Tebar, J.L. Lerma, Á. Marqués-Mateu, Camera characterization for improving color archaeological documentation, *Color Res. Appl.*
36 (2017). doi:10.1002/col.22152.
- 37 [27] C. Roldán, S. Murcia-Mascarós, J. Ferrero, V. Villaverde, E. López, I. Domingo, R. Martínez, P.M. Guillem, Application of field portable
38 EDXRF spectrometry to analysis of pigments of Levantine rock art, *X-Ray Spectrom.* 39 (2010) 243–250. doi:10.1002/xrs.1254.
- 39 [28] B. Ford, J. Druzik, Microfading: the state of the art for natural history collections, *Collect. Forum.* 27 (2013) 54–71.
- 40 [29] T. Lojewski, J. Thomas, R. Golab, J. Kawalko, J. Lojewska, Light ageing with simultaneous colorimetry via fibre optics reflection spectrometry,
41 *Rev. Sci. Instrum.* 82 (2011). doi:10.1063/1.3606645.
- 42 [30] P.M. Whitmore, X. Pan, C. Bailie, Predicting The Fading of Objects: Identification of Fugitive Colorants Through Direct Nondestructive
43 Lightfastness Measurements, *J. Am. Inst. Conserv.* 38 (1999) 395–409. doi:10.1179/019713699806113420.
- 44 [31] R.W.G. Hunt, M.R. Pointer, *Measuring Colour*, Fourth Edi, John Wiley & Sons, 2011. doi:10.1002/9781119975595.
- 45 [32] J. Schanda, *Colorimetry: Understanding the CIE System*, John Wiley & Sons, 2007. doi:10.1002/9780470175637.
- 46 [33] N. Ohta, A. Robertson, *Colorimetry: Fundamentals and Applications*, John Wiley & Sons, 2006. doi:10.1002/0470094745.
- 47 [34] A. Molada-Tebar, J.L. Lerma, Á. Marqués-Mateu, Camera characterization for improving color archaeological documentation, *Color Res. Appl.*
48 43 (2018) 47–57. doi:10.1002/col.22152.
- 49 [35] M. Mahy, L. Van Eycken, A. Oosterlinck, Evaluation of Uniform Color Spaces Developed after the Adoption of CIELAB and CIELUV, *Color*
50 *Res. Appl.* 19 (1994) 105–121.
- 51 [36] D. Malacara, *Color Vision and Colorimetry: Theory and Applications*, Spie Press Book, 2011.
- 52 [37] C.E. Rasmussen, C.K.I. Williams, *Gaussian Processes for Machine Learning*, the MIT Press, London, England, 2006.
- 53 [38] G. Riutort Mayol, Approximate Gaussian processes and derivative information for spatio-temporal regression and classification, *Universitat de*
54
55
56
57
58
59
60
61
62
63
64
65

1
2
3
4
5
6
7
8
9
10
11
12
13
14
15
16
17
18
19
20
21
22
23
24
25
26
27
28
29
30
31
32
33
34
35
36
37
38
39
40
41
42
43
44
45
46
47
48
49
50
51
52
53
54
55
56
57
58
59
60
61
62
63
64
65

València, 2020.

- [39] J. Riihimäki, A. Vehtari, Gaussian processes with monotonicity information, in: Proc. 13th Int. Conference Artif. Intell. Stat., Chia Laguna Resort, Sardinia, Italy, 2010: pp. 645–652. http://machinelearning.wustl.edu/mlpapers/paper_files/AISTATS2010_RiihimakiV10.pdf.
- [40] G. Riutort-Mayol, V. Gómez-Rubio, J.L. Lerma, J.M. del Hoyo-Meléndez, Correlated functional models with derivative information for modeling MFS data on rock art paintings, (2019) 1–14. <http://arxiv.org/abs/1910.12575>.
- [41] J.R. Druzik, Evaluating the Light Sensitivity of Paints in Selected Wall Paintings at the Mogao Grottoes: Caves 217, 98, and 85, in: Conserv. Anc. Sites Silk Road, The Getty, The Getty Conservation Institute, Los Angeles, 2010: pp. 457–463.

1
2
3
4
5 **TABLES**
6
7

8 **Table 1 - Description of the 13 sampling spots surveyed with the MFT device.**

9

Spot number	Description	Type of pigment
1	A human figure, area of torso, red-painted and light brown substrate. Not integrated into the hunting scene,	Red pigment.
2	Orange rock-substrate.	-
3	Hunter leg in dark red painting. Human figure integrated into the hunting scene.	Dark red pigment.
4	Hunter hand in dark red painting. Corresponds to the same representation as to the sample 3	Dark red pigment.
5	Hunter leg in red painting. Not integrated into the hunting scene.	Red pigment on an orange-pink substrate.
6	Red zone boar's rump next to an area of the orange-pink substrate. Integrated into the hunting scene.	Red pigment.
7	Red zone on the big wild boar figure. Integrated into the hunting scene.	Red pigment.
8	Orange substrate	-
9	Light brown substrate.	-
10	Substrate flaked	-
11	Orange-reddish substrate	-
12	Hunter leg in dark red painting. Integrated into the hunting scene.	Dark red pigment.
13	Light orange substrate.	-

10
11
12
13
14
15
16
17
18
19
20
21
22
23
24
25
26
27
28
29
30
31
32
33
34
35
36
37
38
39
40
41
42
43
44

45 **Table 2 - Summary statistics of the input variables.**

	H	S	I	x	y
Mean	5.255	9.704	5.155	3.549	4.969
Std. Dev.	1.0	1.0	1.0	0.732	0.674
1st Qu.	4.359	9.042	4.603	2.910	4.387
3rd. Qu.	5.913	10.273	5.772	4.187	5.551

46
47
48
49
50
51
52
53
54
55
56
57
58
59
60
61
62
63
64
65

Table 3 - Description of the spots analyzed.

Spot number	Description	Type of sample	Pixel color (t=11)
1	Torso of a human figure. (Not integrated into the hunting scene)	Red pigment	Dark red pixel
2	Animal head figure. (Integrated into the hunting scene)	Dark red pigment	Dark orange pixel
3	Hunter head in dark red painting. (Not integrated into the hunting scene)	Dark red pigment	Dark red pixel
4	Animal leg of the central figure in dark red painting. (Integrated into the hunting scene)	Dark red pigment	Dark red pixel
5	Light brown substrate.	Rock-support	Blue pixel

FIGURE CAPTIONS

Fig.1. View of Cova Remigia from the entrance.

Fig. 2. Cova Remigia: a) View of the shelter number V and sampling spots cross-marked; b) Sampling spots evaluated with the MFT setup.

Fig. 3. Chromaticity diagram of the 13 sampling spots.

Fig. 4. MFT data acquisition on site.

Fig. 5. Predictive means (solid line) and 95% pointwise credible intervals (dotted line), superimposed to the MFT observed measurements (cross points) based on color differences.

Fig. 6. Predictive means (solid line) and 95% pointwise credible intervals (dotted line), superimposed to the MFT observed measurements (cross points) based on chroma differences.

Fig. 7. Estimation of the spectral response change based on color differences ΔE_{ab}^* for times t=3, 4, 5, 6, 8, and 11. (Taken from [40]).

Fig. 8. Estimation of the spectral response change based on chroma differences at different times (t=3, t=4, t=5, t=6, t=8, t=11).

Fig. 9. Selection of spots: chroma difference (t = 11).

Fig. 10. Tracking of the 5 selected spots (Fig. 9) over time.

Figure 1



Figure 2a

[Click here to access/download;Figure;fig2a.JPG](#)



Figure 2b

[Click here to access/download;Figure;fig2b.jpg](#)

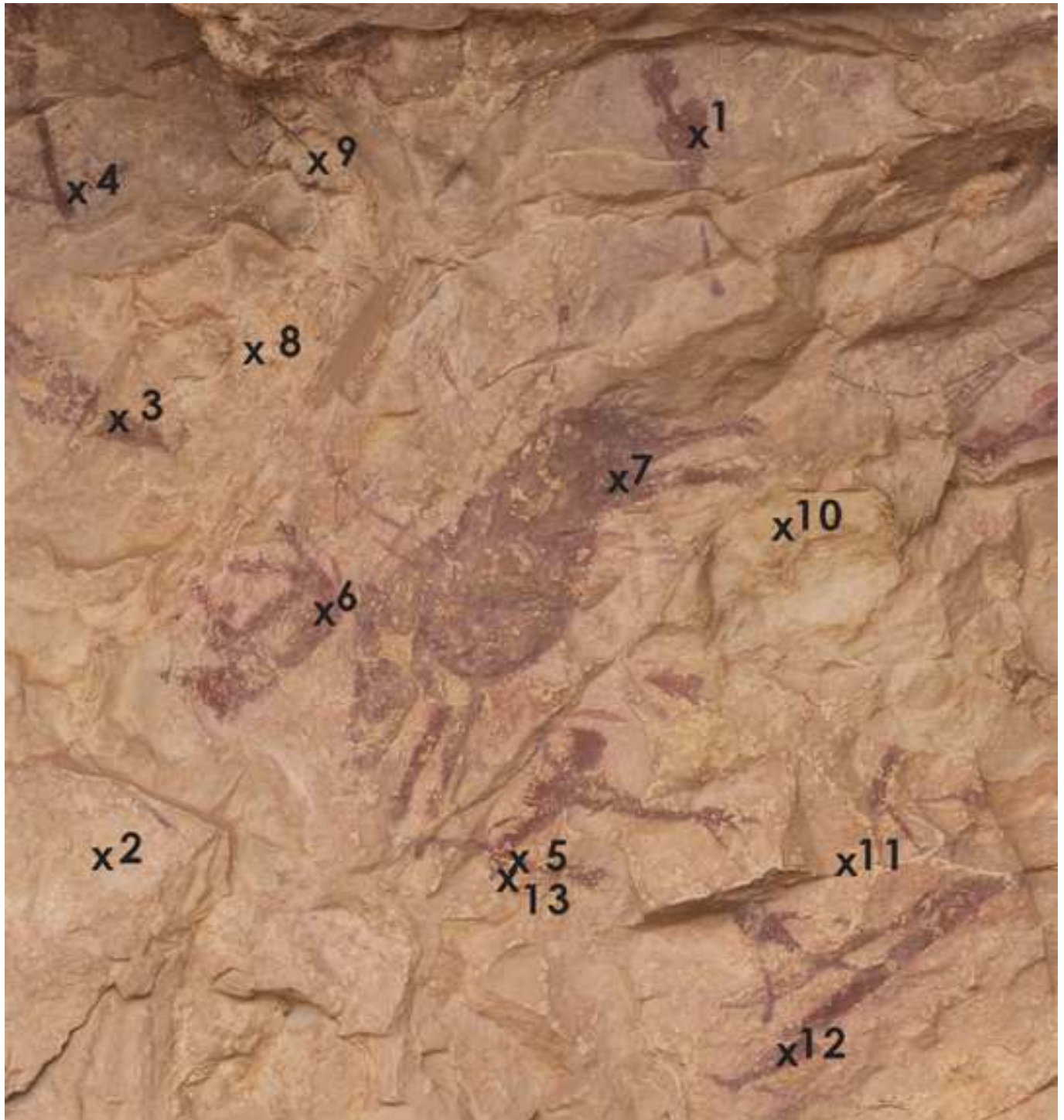


Figure 3

[Click here to access/download;Figure;fig3.jpg](#)

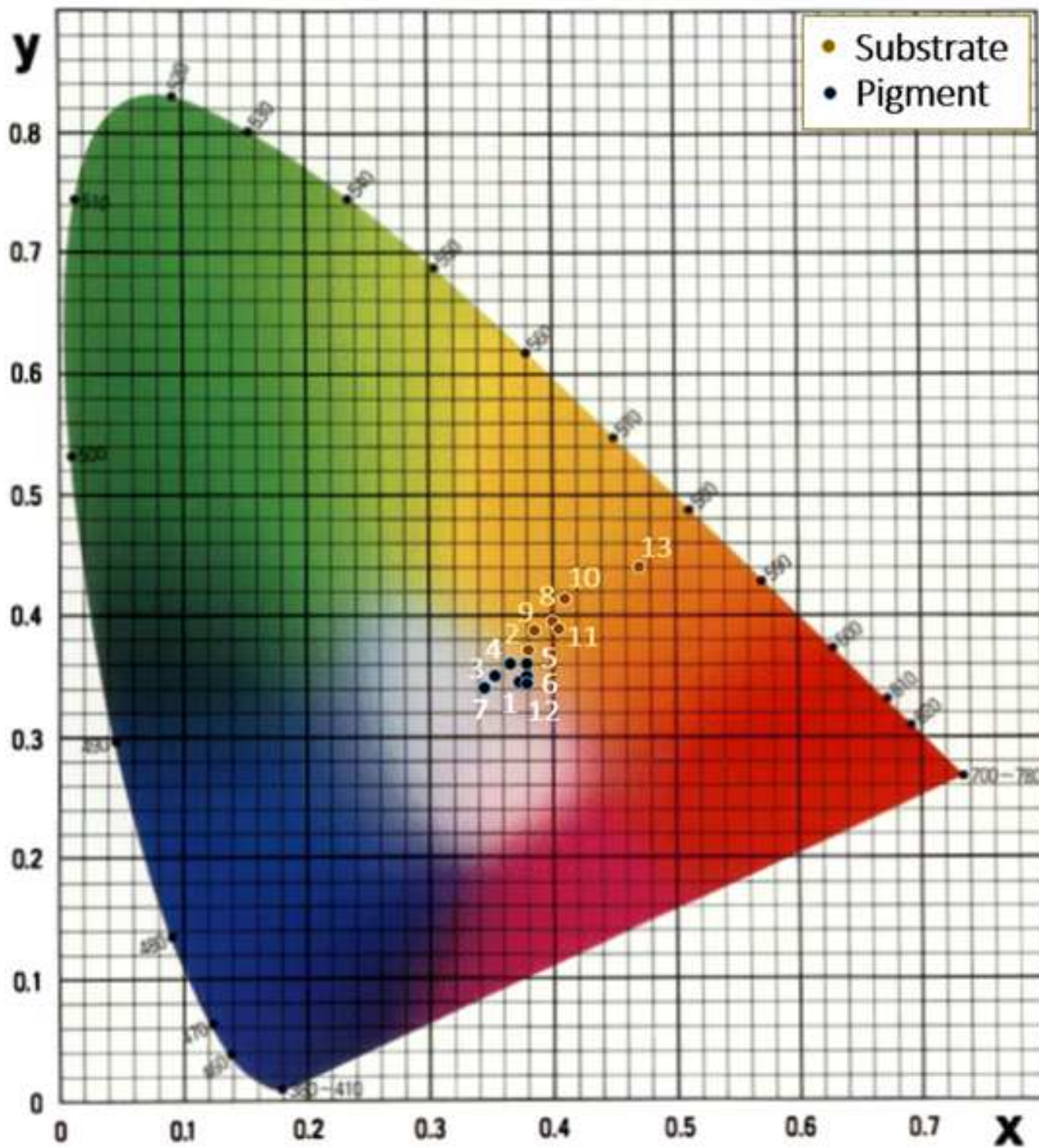


Figure 4



Figure 5

[Click here to access/download;Figure;fig5.jpg](#)

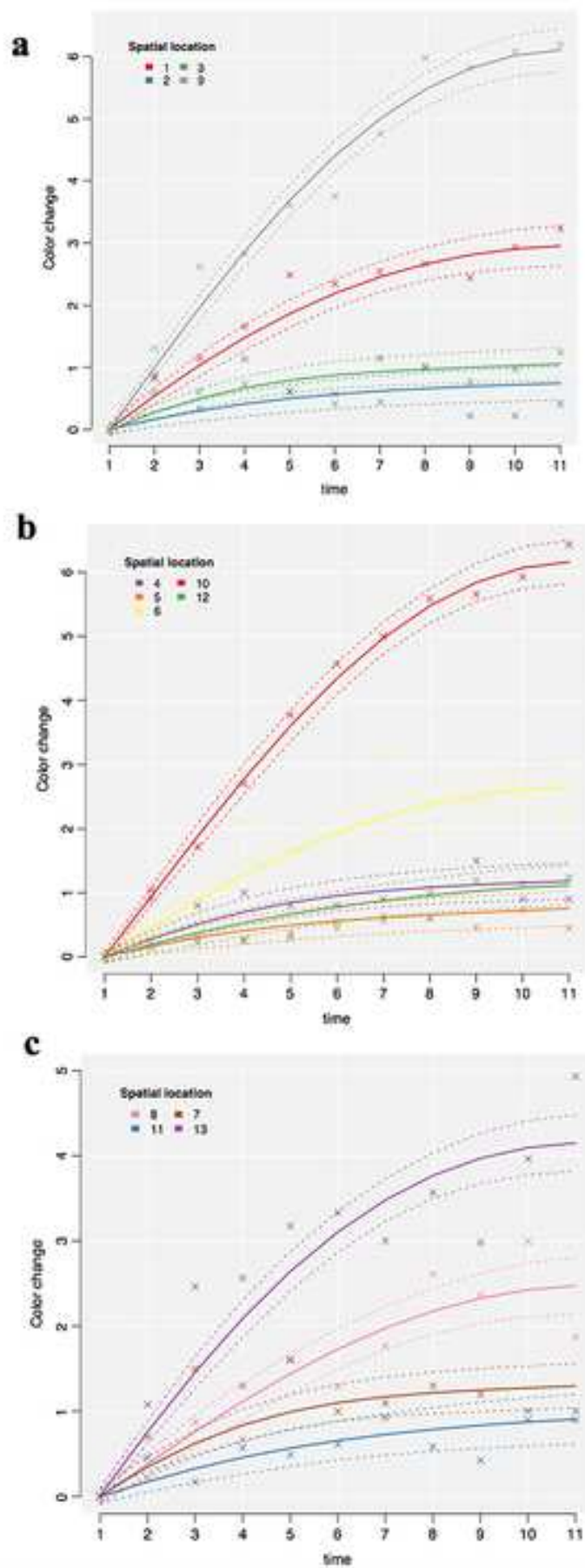
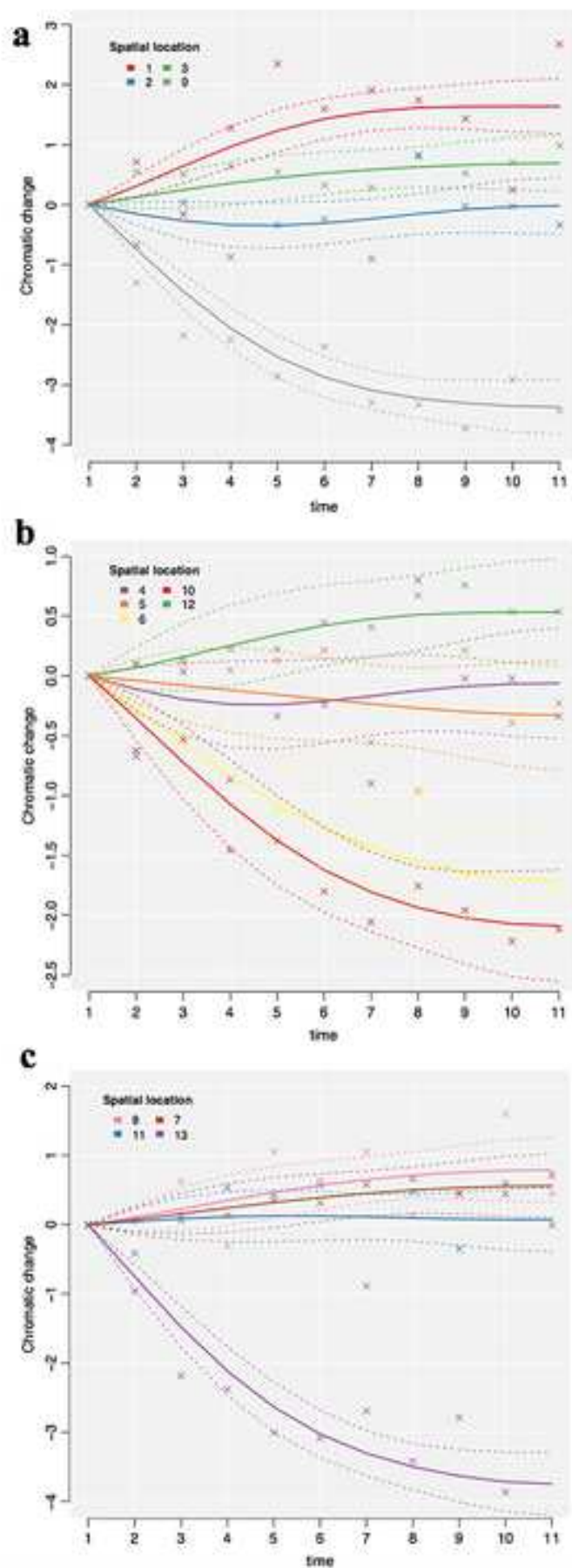
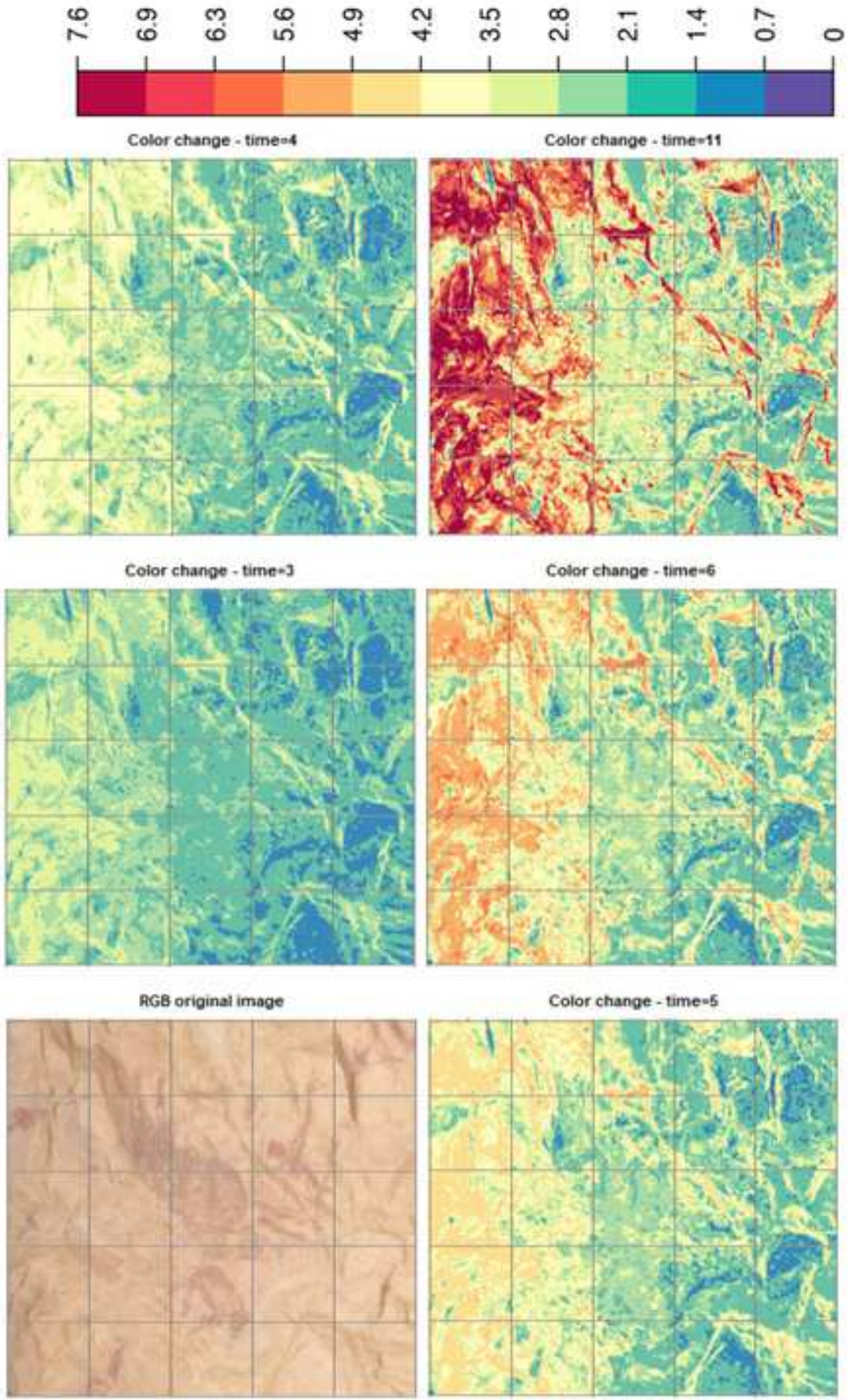


Figure 6

[Click here to access/download;Figure;fig6.jpg](#)





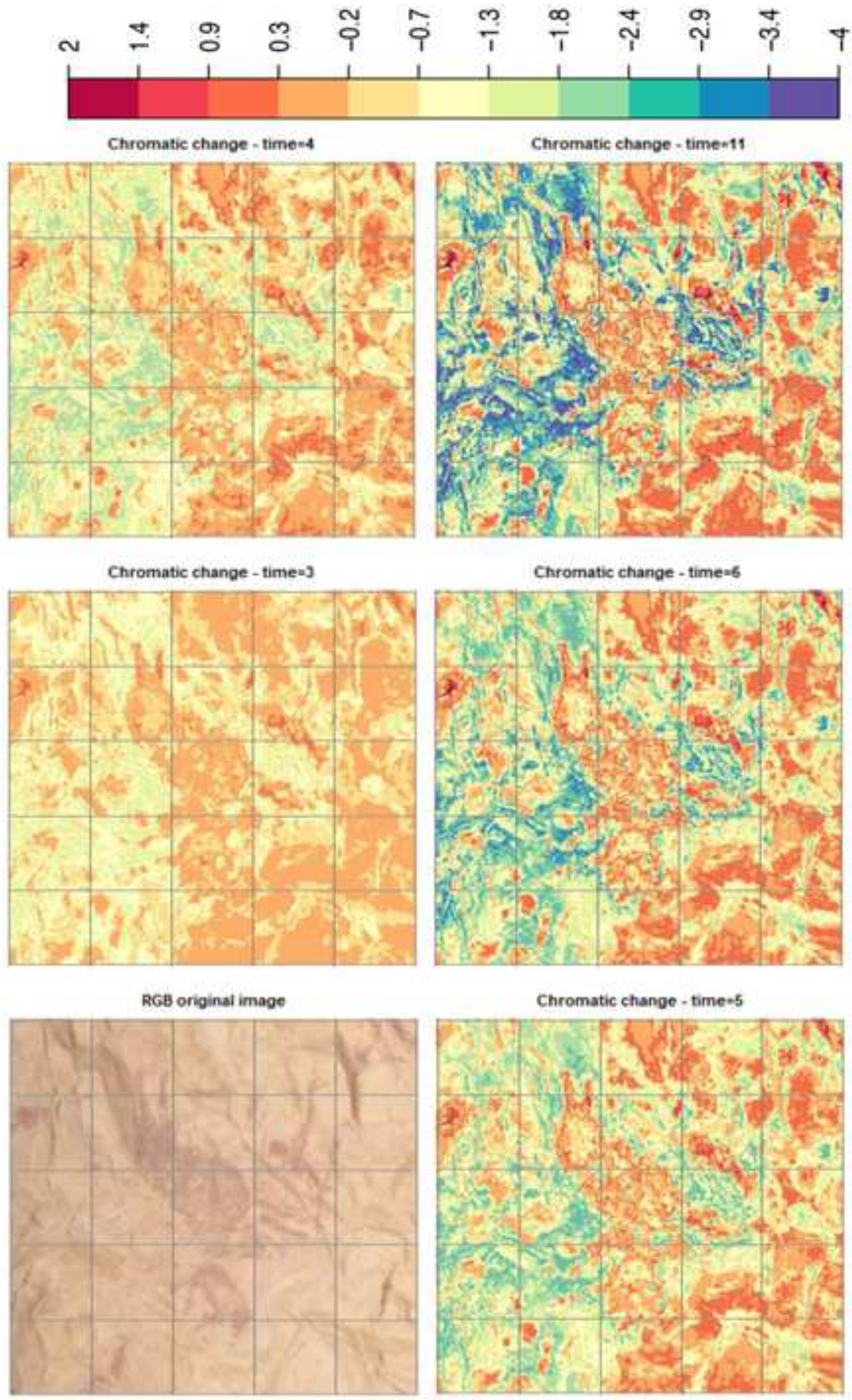


Figure 9

[Click here to access/download;Figure;fig9.jpg](#)

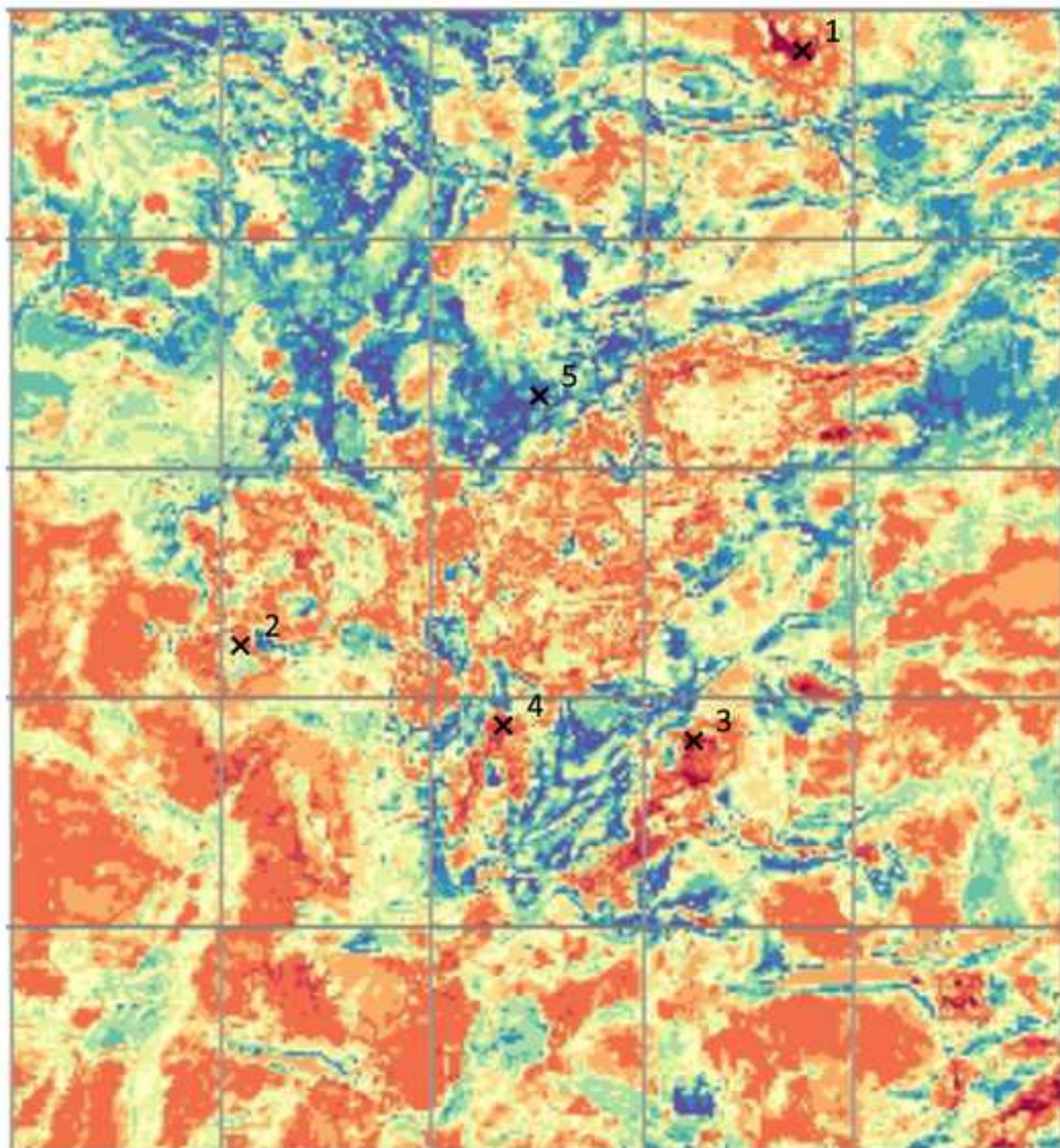
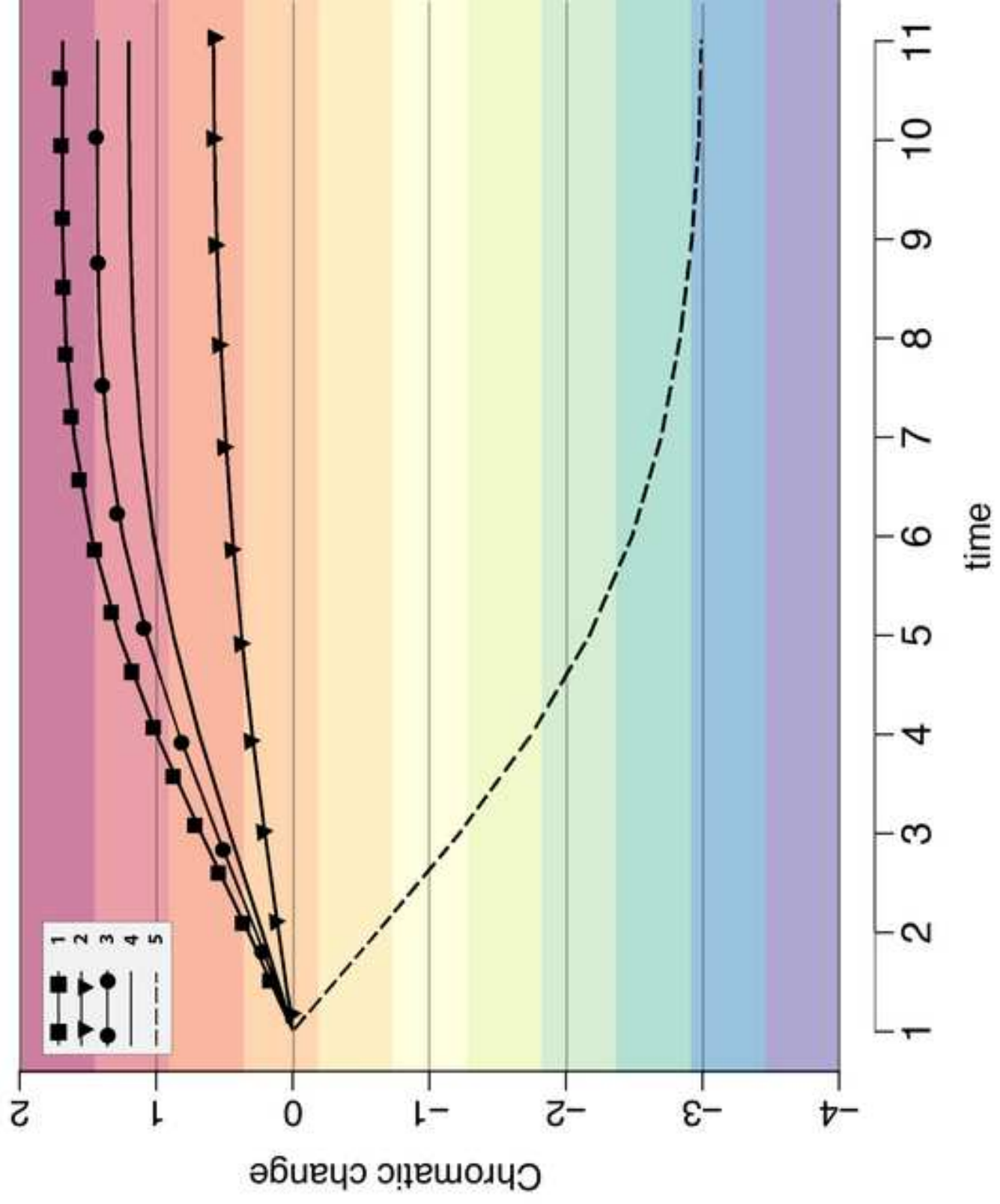



Figure 10

[Click here to access/download;Figure;fig10.jpg](#)



Table



[Click here to access/download](#)

Table

Tables_01.docx

